

RESEARCH ARTICLE | APRIL 24 2024

# Plasma-enhanced chemical vapor deposition a-SiOCN:H low-Z thin films for bulk acoustic wave resonators

Claudio Berger ; Michael Schneider ; Georg Pfusterschmied ; Ulrich Schmid 



*J. Appl. Phys.* 135, 165304 (2024)

<https://doi.org/10.1063/5.0197261>



Journal of Applied Physics

Special Topics Open  
for Submissions

[Learn More](#)



# Plasma-enhanced chemical vapor deposition a-SiOCN:H low-Z thin films for bulk acoustic wave resonators

Cite as: J. Appl. Phys. **135**, 165304 (2024); doi: [10.1063/5.0197261](https://doi.org/10.1063/5.0197261)

Submitted: 12 January 2024 · Accepted: 8 April 2024 ·

Published Online: 24 April 2024



Claudio Berger,<sup>a)</sup> Michael Schneider, Georg Pfusterschmied, and Ulrich Schmid

## AFFILIATIONS

Institute of Sensor and Actuator Systems, TU Wien, Gusshausstrasse 27-29, 1040 Vienna, Austria

<sup>a)</sup>Author to whom correspondence should be addressed: [berger2claudio@gmail.com](mailto:berger2claudio@gmail.com)

## ABSTRACT

The 5th generation (5G) wireless telecommunication standards with newly defined frequency bands up to 6 GHz are currently established around the world. While outperforming surface acoustic wave (SAW) filters above 1 GHz, bulk acoustic wave (BAW) resonators in multiplexers for radio-frequency front-end (RFFE) modules continuously face higher performance requirements. In contrast to free-standing bulk acoustic resonators (FBARs), solidly mounted resonator (SMR) technology uses an acoustic Bragg mirror, which has already been successfully applied for several GHz applications. In this work, we investigate the potential of amorphous hydrogenated silicon-oxycarbonitride (a-SiOCN:H) thin films synthesized with low-temperature *plasma-enhanced chemical vapor deposition* (PECVD) as a low acoustic impedance (low-Z) material. Compared to the state-of-the-art where in Bragg mirrors up to now SiO<sub>2</sub> is used as standard, the acoustic impedance ratio against the high-Z material tungsten (W) is enhanced for a better device performance. To limit the expected increase in viscous loss when the acoustic impedance is reduced, to a minimum, predominantly the mass density was reduced while keeping the mechanical elasticity high. By doing so, acoustic impedance values as low as 7.1 MRayl were achieved, thereby increasing the impedance ratio of high-Z to low-Z materials from 8:1 up to 14:1.

07 November 2024 11:08:36

© 2024 Author(s). All article content, except where otherwise noted, is licensed under a Creative Commons Attribution (CC BY) license (<https://creativecommons.org/licenses/by/4.0/>). <https://doi.org/10.1063/5.0197261>

## I. INTRODUCTION

Bulk acoustic wave (BAW) resonators have recently turned out to be indispensable for high-performance radio-frequency front-end (RFFE) module applications, latest since it came to advanced connectivity standards such as UMTS/WCDMA (3G), LTE (4G), or currently 5G, as well as their mutual coexistence. Complex antenna systems and high-level system-integrated RF modules are required, which continuously demand further miniaturization.<sup>1,2</sup> Previously applied acoustic filtering focused on surface acoustic wave (SAW) technology due to its simple device implementation. As a consequence, until today, SAW is the technology of choice for applications operated at frequencies up to 1 GHz. However, when increasing the frequency further into the mid-bands (<6 GHz), as is currently rolled out all over the world through 5G standards,<sup>3</sup> SAW is no longer preferred due to an enhanced power consumption that is disadvantageous as power amplifiers become less efficient at higher frequencies and energy losses, in general, need to be minimized for

mobile applications.<sup>1</sup> Instead of BAW, the simple film thickness reduction approach following the  $\sim 1/f$  rule<sup>1</sup> to increase filter frequencies is valid even for high power levels.

When looking at BAW technology, two different concepts of either free-standing bulk acoustic resonators (FBARs) or solidly mounted resonators (SMRs) are the standard.<sup>4</sup> FBARs basically consist of a free-standing piezoelectric thin film sandwiched between the top and bottom metal electrodes forming a cavity underneath. This structure traps the acoustic waves that are generated from the piezoelectric film by isolation through air interfaces on both sides. In contrast, SMRs only feature one air interface above the top metal electrode. Beneath, they instead use an acoustic Bragg mirror, isolating the bottom electrode from the carrier substrate to avoid energy leakage into the bulk. The principal structure of this acoustic crystal (Bragg mirror) is the alternation of material domains by a multilayered stack of thin films with high and low acoustic impedances. By internal wave reflections at the respective material interfaces due to

acoustic impedance steps, interference is exploited to minimize acoustic energy transfer into the bulk, thereby providing acoustic isolation. As the ratio between the acoustic impedances of the respective materials is increased, the reflectivity of the Bragg mirror can be enhanced. Key parameters to quantify the performance of BAW devices are the *effective coupling coefficient* ( $k_{\text{eff}}^2$ ) as a measure on how efficiently the energy is converted between the electric and acoustic domain or the *quality factor* ( $Q$ ) as a general measure for resonators. Both quantities can be optimized individually by the design of an acoustic reflector stack, whereas often their product is quantified as the *figure of merit* ( $FOM$ ).

As SMR technology features the acoustic Bragg mirror, the mechanical stress field induced in the multilayered structures always causes a decrease in coupling compared to FBARs.<sup>3</sup> In addition, acoustic losses within the different materials reduce  $Q$ , especially the low- $Z$  oxide layers due to their much smaller elasticity in comparison to the high- $Z$  materials.<sup>5</sup> The main features to prefer SMR instead of FBAR are the increased mechanical robustness, their process reliability, and thereof its resulting long-term stability. Furthermore, the understanding of acoustic dispersion strongly increased the performance of SMR technology.<sup>6,7</sup>

To overcome the mentioned drawbacks in SMR devices, research about tailored low- $Z$  materials with a reduced acoustic impedance  $Z$ , a property that is directly dependent on the mass density and the mechanical elasticity (*Young's modulus*) is of utmost importance. The goal of these efforts is to decrease  $Z$  in low- $Z$  materials to a minimum or at least below the value of standard  $\text{SiO}_2$  of 13 MRayl, in order to increase the impedance ratio between low- $Z$  and high- $Z$  materials for an enhanced mirror reflectivity in a certain frequency range. Recent attempts to reduce the acoustic impedance of the mainly used  $\text{SiO}_2$  focused on pulsed DC sputtering forming a less-dense, porous microstructure to reach lower mass densities.<sup>8,9</sup> Other approaches were based on thin films for coupled resonator filters (CRF) where the incorporation of carbon led to a porous material microstructure referred to as carbon-doped oxide (CDO),<sup>10–13</sup> organo-silicate glass (OSG), or silicon-oxycarbide (SiOC, SiOCH) in combination with SMRs.<sup>14</sup> Besides these experimental efforts, SiOC has also been the focus of theoretical investigations.<sup>15</sup> In general, SiOC has been thoroughly investigated as a material system, originating from the field of low- $k$  interlayer dielectrics (ILD)<sup>16–18</sup> starting in the 90s. Their investigation was driven by the basic idea that such thin films possess decreased mass densities and, hence, reduced acoustic impedances due to the presence of pores within these material systems. For low- $k$  applications, the porosity delivers polarization-free zones or voids, but for low- $Z$  applications, viscous losses emerge due to mechanical softening. These pores originate during the fabrication process from the use of specific organo-silicate precursors as, e.g., trimethylsilane (TMS) or others with a similar chemical composition.<sup>19,20</sup> Another step toward reaching even lower dielectric constants was taken by co-deposition of porogen precursors that were later removed in either a post-annealing or UV-curing step, leaving porosities of up to 50%.<sup>16</sup> To overcome the simultaneous mechanical weakening within these materials, pre-defined bond structures within complex precursors were introduced and tried to be directly transferred into the *as-deposited* films.<sup>18</sup>

In terms of acoustic performance, this mechanical softening is disadvantageous, and accordingly, the achieved low acoustic impedances of 2–11 MRayl are accompanied by relatively high attenuation coefficients  $\alpha$  of 300–5000 dB/cm, even at only 1 GHz,<sup>11</sup> compared to  $\sim 10$  dB/cm for standard  $\text{SiO}_2$ . Acoustic attenuation can be understood as a generalized loss mechanism within acoustic media and is by theory directly dependent on the frequency  $\omega$  but also on several other material parameters such as the sound velocity  $v \approx \sqrt{c/\rho}$  of the material, which itself again depends on the *Young's modulus* ( $c$ ) and the mass density  $\rho$  as well as the material viscosity  $\eta$ .<sup>21</sup> From these basic considerations, it is obvious that the reduction in the acoustic impedance through a lowered mass density leads to a decreasing elasticity, which, in turn, however, enhances wave propagation losses.

It is the objective of this work to develop an optimized material deposition technology for CMOS-compatible low- $Z$  layers fulfilling the contrary requirements for a lowered mass density while keeping the *Young's modulus* as high as possible. To the best of the authors' knowledge, this technical challenge with competing material-related objectives to replace dense  $\text{SiO}_2$  in high-frequency acoustic Bragg mirror applications with another low acoustic impedance material system has not been achieved so far.

## II. EXPERIMENTAL DETAILS

The method of choice to produce low- $Z$  thin films is *plasma-enhanced chemical vapor deposition* (PECVD) due to its broad range of dielectric materials that can be deposited. As a facility, an *Oxford 100 Plasmalab* was used (see Fig. 1), which offers a large variability for all necessary deposition parameters. To avoid perpendicular acceleration of particles toward the substrate, the chamber is wrapped with a spiral coil wire leading to circular electric field lines that excite the plasma by a frequency of 13.56 MHz. Two different valves control the supply of either argon (Ar) and nitrous oxide ( $\text{N}_2\text{O}$ ) or closer to the substrate surface the precursor gas flow of silane ( $\text{SiH}_4$ ) and methane ( $\text{CH}_4$ ). Furthermore, the chamber pressure as well as the substrate temperature can be varied.

### A. Deposition parameters

In a first screening, the gas flows of the reactive precursors were varied over 35 depositions with a fixed total gas flow rate of 20 SCCM. In doing so, a whole set of amorphous dielectric material systems in combination with silicon were realized and characterized. The deposited thin films ranged from pure silicon (a-Si) when only silane was used as a precursor and toward further matrices in the directions of silicon nitride (a-SiN<sub>x</sub>), silicon oxide (a-SiO<sub>x</sub>), and silicon carbide (a-SiC<sub>x</sub>) or even a mixture of all. Through thin film characterization, advantageous properties for low acoustic impedance evolved by a certain group of depositions when following the black line in Fig. 2 from silicon oxides to carbides. These in-between compositions can be described as amorphous silicon oxy-carbo-nitrides (a-SiO<sub>x</sub>C<sub>y</sub>N<sub>z</sub>) when partially exchanging  $\text{N}_2\text{O}$  with  $\text{CH}_4$  and remaining is the precursor flow of  $\text{SiH}_4$  constant. All depositions were made on 4" polished Si wafers with a thickness between 300 and 1000 nm.

In a second screening comprising 15 deposition runs, the focus was on the impact of physical parameters such as chamber pressure,

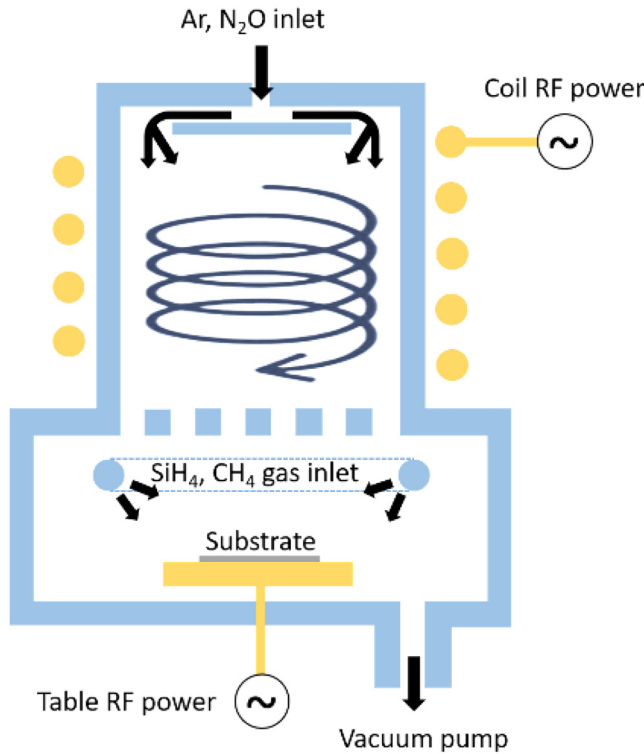


FIG. 1. Schematic cross-sectional view on the PECVD facility.

substrate temperature, Ar gas flow, or total plasma power. These parameters were varied toward a generalized optimum for lowered mass densities and the highest possible mechanical strength for the advantageous focal point of 6 SCCM SiH<sub>4</sub>, 4 SCCM N<sub>2</sub>O, and 10 SCCM CH<sub>4</sub> (referenced as a-SiOCN:H) obtained from the first screening. After this second screening, all the optimized parameters for a low acoustic impedance (low-density) thin film are listed in Table I. The optimized parameters were then applied to a defined set of eight precursor compositions along the line of constant silane gas flow (6 SCCM) forming differing types of a-SiO<sub>x</sub>C<sub>y</sub>N<sub>z</sub>:H (and a-SiO<sub>2</sub>:H as a reference) for direct comparison of several low-density thin film matrices, through a partial exchange of N<sub>2</sub>O (from 14 SCCM down to 0) with CH<sub>4</sub> (from 0 to 14 SCCM).

Post-deposition treatment involved *rapid thermal annealing* (RTA) in an oven in a nitrogen (N<sub>2</sub>) atmosphere at 1 mTorr for 1h at 450 °C, to investigate modifications of the thin films when exposed to elevated temperatures, which arise in subsequent BAW manufacturing processes.

### B. Characterization methods

Several methods were applied to investigate the deposited thin films for advantageous properties as low-Z materials. The crucial figure of interest for the design of an acoustic Bragg mirror within

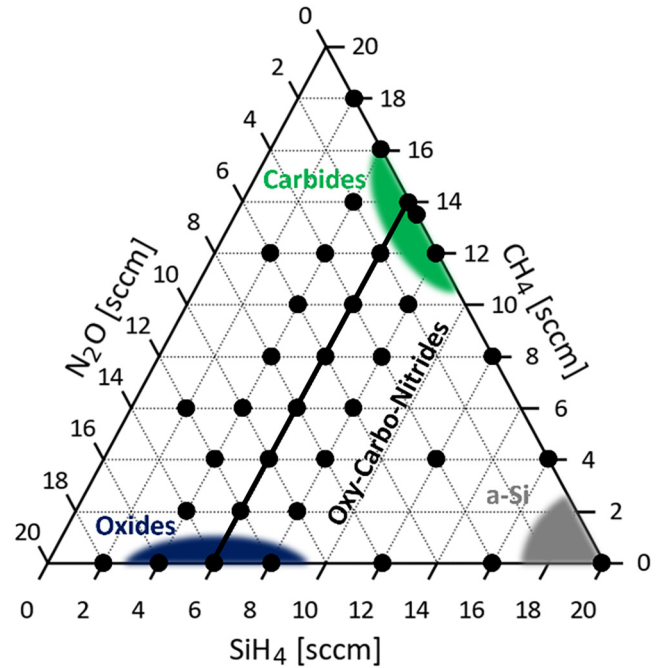


FIG. 2. The ternary diagram of the precursor gas composition, whereas the black dots represent the precursor gas concentrations of different thin film depositions. With vanishing SiH<sub>4</sub> content, the deposition rate also reduced toward 0. Specifically, the region between the silicon oxides and carbides proved to be advantageous for the synthetization of thin films with low acoustic impedance.

a BAW resonator is the acoustic impedance,<sup>21</sup>

$$Z = \sqrt{\rho c}, \quad (1)$$

which is directly dependent on the mass density  $\rho$  as well as Young's modulus  $c$ . An exact determination of mass densities required the measurement of according film thicknesses of the low-Z dielectric material systems. In this work, *optical reflectometry* (OR) was used as a non-destructive method to characterize pre- and post-annealed thin films with a *Filmetrics F20-UVX Spectral Reflectometer*. Hereby, a perpendicularly incident light beam is reflected on the sample surface as well as the film interface to the substrate for a wavelength-dependent interference pattern. The used wavelengths ranged from 400 to 800 nm. From interference maxima, film thickness as well as the *refractive index* of the material are determined by a model fit.

TABLE I. Optimized deposition parameters for low mass densities.

Parameter	Standard	Optimized
ICP power (W)	1500	300
Chamber pressure (mTorr)	6	20
Substrate temperature (°C)	250	0
Ar gas flow rate (sccm)	0	50

07 November 2024 11:08:36

With the help of this method, the deposited film thickness was mapped on the 4" Si wafer to obtain the total film volume for exact mass density calculations.

These results with respect to the film thickness were compared to cross-sectional analyses performed with *scanning electron microscopy (SEM)* from *Hitachi (SU8030)* operated at an acceleration voltage of 15 kV.

The weight for the mass density calculation was obtained by pre- and post-deposition wafer mass weighing of the 4" Si wafers with a microbalance of the type *SI-234A* from *Denver Instruments* having a resolution of 10  $\mu\text{g}$ .

Confirmation for the mass density was achieved by the highly precise method of *X-ray reflectometry (XRR)*, performed at the wavelength of the  $\text{Cu-K}\alpha_1$  line. Hereby, an x-ray beam with grazing incidence is reflected by the sample surface, starting from an angle of  $0^\circ$ . When having low surface roughness and low substrate bow, the x-ray beam is reflected until the critical angle is reached from where the beam starts to penetrate into the thin film surface, thus decreasing the intensity of the reflected beam.

The interface step in the mass density of the thin film material toward air is directly related to the critical angle, where reflection turns into penetration.

The other important material parameter is *Young's modulus*, which is directly linked to the sound velocity. A very straightforward method used in this work was *nanoindentation*, where a hardened tip is mechanically forced into the thin film in the perpendicular direction, recording the applied force as a function of the penetration depth. For this purpose, a *Fischer-Cripps Laboratory UMIS* equipped with a *Berkovich* diamond tip indenter was applied for thin films of nominally 1  $\mu\text{m}$  thickness. The maximum indentation force was 45 mN. As this measurement method is independent of a certain material model, a relative comparison of thin films with differing compositions can be performed on a qualitative level. The load-displacement curves were evaluated according to the *Oliver-Pharr Method*.<sup>22</sup>

Compared to this rather static method, sound velocity measurements were also performed by *picosecond ultrasonic* (see Fig. 3). By this method,<sup>23,24</sup> a pulsed laser locally creates oscillating thermal expansions on the surface of the investigated thin film. Due to this local, structural expansion, an acoustic pressure wave propagates into the material perpendicular to the surface that is partially reflected on the bottom interface. This reflected acoustic wave front can be detected by an optical reflectivity change  $\Delta R$  by probing the surface with another laser, which directly records the time of propagation through a distance of twice the film thickness. Multiple signals from reflected waves of other interfaces may also be detected since the investigated thin film was directly deposited as the low-Z layer in the uppermost mirror pair of a *Bragg reflector*. To avoid any chemical reactions through direct contact of the heated laser spot at carbon-containing residues on the thin film surface with air, a thin capping layer of 100 nm AlCu was deposited on top of the 800 nm low-Z material thin film prior to the characterization.

Another important material parameter is the residual layer stress  $\sigma$  of the a-SiOCN:H thin films. Investigations were again performed on 4" Si wafers by a capacitive measurement technique applying equipment from *E + H Metrology MX203-6-33*, offering a resolution of 100 nm in wafer bow determination, which is indirectly

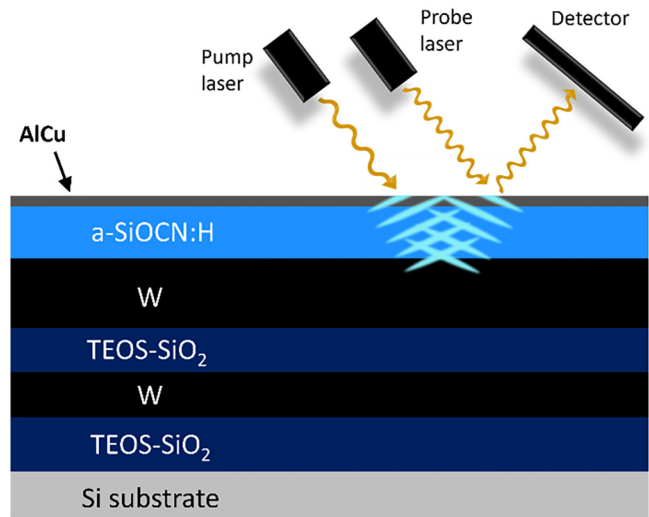


FIG. 3. Schematic of the picosecond ultrasonic measurement method for the determination of the sound velocity in a low-Z thin film. Reflections from other interfaces within the stack may also be detected.

proportional to the curvature radius  $R_c$ . From the latter parameter, the residual film stress is determined by the *Stoney equation*,<sup>25</sup>

$$\sigma = \frac{M t_s^2}{6 R_c t_f}, \quad (2)$$

with the biaxial modulus  $M$  of the substrate and the thicknesses of the substrate  $t_s$  and of the thin film  $t_f$ , respectively. The chemical composition was measured with *x-ray photoelectron spectroscopy (XPS)* using monochromatic  $\text{Al-K}\alpha$  radiation in an *ESCALAB 250 Xi* from *Thermo Fisher Scientific*. Prior to any analysis, Ar ion etching with a *MAGICS*-ion source was performed to remove any residues or chemical contamination from the sample surface.

Finally, *Fourier transform-infrared spectroscopy (FT-IR)* is performed with a *Bruker Tensor* for chemical analysis by recording the molecular vibration spectrum in the wavenumber range of  $400\text{--}4000\text{ cm}^{-1}$  known as the mid-IR spectrum. Preliminary calibration measurements were undertaken on pure 4" Si wafers and subtracted subsequently from the samples with deposited thin films to obtain the pure transmission spectrum of the materials investigated. The transmission spectra were normalized by their film thickness, resulting in a spectrum of the *absorption coefficient*. Additionally, a polynomial baseline correction was performed.

### III. RESULTS AND DISCUSSION

In PECVD, a steady glow discharge plasma serves as an energy source for precursor decomposition enabling comparably low deposition temperatures making it suitable for *back end of line (BEOL)* processing with high reproducibility.<sup>26</sup> As standard precursor gases for  $\text{SiO}_2$ , the combination of silane ( $\text{SiH}_4$ ) and some oxygen containing precursor like nitrous oxide ( $\text{N}_2\text{O}$ ) is used, generally resulting in

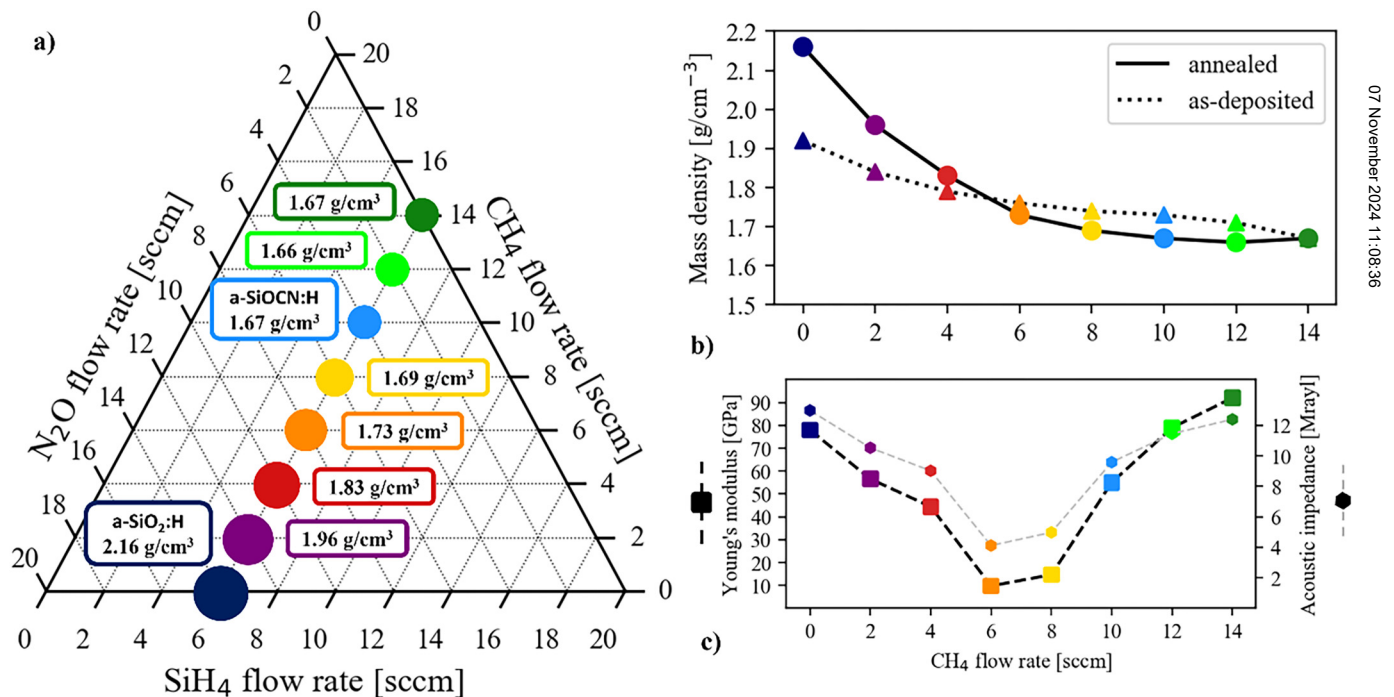
amorphous hydrogenated silicon oxide thin films ( $a\text{-SiO}_2\text{:H}$ ). Thereby, silane not only introduces Si atoms as the main element but also a certain amount of hydrogen terminations, whereas the nitrous oxide likely decomposes into volatile  $\text{N}_2$  and highly reactive oxygen radicals for thin film formation.<sup>27</sup> If the correct ratio of precursor gases is chosen, a highly stoichiometric but hydrogenated  $a\text{-SiO}_2\text{:H}$  is produced, which is also used as a reference material system in this work. As an effect of altered deposition parameters for this process, the incorporation of nitrogen has to be considered within the aspect of chemical composition, generally speaking of  $a\text{-SiON:H}$  thin films.

Another material system for which PECVD has proven to be beneficial is amorphous hydrogenated silicon carbide ( $a\text{-SiC:H}$ ), formed by the use of  $\text{SiH}_4$  together with methane ( $\text{CH}_4$ ) as precursor gases. Again, hydrogen terminations are introduced by both precursors and the deposited  $a\text{-SiC:H}$  shows similar mass densities compared to oxides, although with a higher mechanical stability indicated by enhanced Young's moduli up to 200 GPa.<sup>28–30</sup>

To find a material system that combines low mass density and high mechanical stability, the simultaneous deposition of both oxide and carbide resulting in  $a\text{-SiOCN:H}$  was considered as promising approach. The incorporation of carbon through the

corresponding methyl groups ( $-\text{CH}_x$ ) is proven to result in low-density material characteristics as also known from prior SiOC research,<sup>17,18,31</sup> whereas the simultaneous introduction of stronger Si-C bonds may result in an increased Young's modulus. By selecting precursors of the simplest molecular structure for the *as-deposited* films, a chemically homogenous and amorphous material system is synthesized, which avoids the generation of pores.

One crucial aspect when it comes to integration is the thermal stability of the developed material composition.  $\text{SiO}_2$  has proven to be stable also at high thermal stresses during the manufacturing process. In terms of BAW, the critical temperature is the one for the sputtering process of the piezoelectric thin film, which is aluminum nitride (AlN) or aluminum scandium nitride (AlScN), at around 400–450 °C. Hence, for the low-Z layers in this paper, thermal stability is required for process temperatures up to this range. The following results presented will thereby always regard *annealed* thin films, instead of *as-deposited* if nothing else is stated. To describe the development path within the pre-defined set of eight variations in the precursor composition comprising depositions from oxide toward carbide thin films, the reference matrix of  $a\text{-SiO}_2\text{:H}$  with optimized deposition parameters serves as the starting point, which can be seen in the ternary diagram of Fig. 4.



07 November 2024 11:08:36

**FIG. 4.** (a) Defined set of eight depositions with modification of the precursor gas flows for low-density thin film synthesis. In (b), the mass density decreases when moving away from the reference and toward the carbide region, with a strong dependency on RTA treatment. In contrast to the compositions close to the reference, which experienced oxide densification and thereby a reduction in film thickness through RTA, the thin films with moderate to high  $\text{CH}_4$ -precursor gas flows showed a slightly enhanced film thickness. In (c), Young's moduli were only obtained by nanoindentation on annealed thin films, stating a clear trend for decreasing elasticity when leaving the oxide-rich compositions, but enhanced elasticity as moving toward carbides, despite of a comparably low mass density. Hence, a corresponding trend for the acoustic impedance can be assumed based on the development of Young's modulus. The focal point of  $a\text{-SiOCN:H}$  emerged representing an optimized trade-off between low acoustic impedance and an elasticity as high as possible for low viscous loss.

The mass density was measured before and after post-deposition annealing with a strong dependency on the precursor gas flow composition. For little or no  $\text{CH}_4$  gas flows within the precursor composition, the film thickness substantially decreased after exposure to elevated temperatures, whereas this behavior reversed when entering the region of moderate and high  $\text{CH}_4$ -precursor content. Obviously, the low-density film growth is highly sensible toward thermal activation, thus leading to two possible scenarios, based on the atomic content available by the *as-deposited* matrix. In the reference film without any C atoms as well as in compositions deposited with low  $\text{CH}_4$  precursor gas flows, the thermal energy applied within the *RTA* led to an outgassing of H, leaving a densified oxide-rich thin film. For samples with moderate to high  $\text{CH}_4$  gas flow, the thin films also outgassed H but were dominated by another thermal effect that can be assumed as structural healing with a slight expansion of up to 3% in film thickness. Thus, in combination with the obtained mass reduction by outgassing, this effect led to a decrease in the mass densities. Young's modulus was obtained merely on annealed thin films by *nanoindentation*, clearly trending the decrease in elasticity when departing from the reference  $\text{a-SiO}_2\text{:H}$  into a region of high oxide-carbide mixture. As the content of  $\text{CH}_4$  flow is enhanced toward carbide-rich films, also Young's modulus increases strongly, going beyond the value for typical oxides when reaching  $\text{a-SiC:H}$  thin films with values of 90 GPa and above. Considering the trade-off between high as possible elasticity (for low viscous loss) and low acoustic impedance (for high reflectivity), the focal point emerged as an optimized composition with a mixture of 6 SCCM  $\text{SiH}_4$ , 4 SCCM  $\text{N}_2\text{O}$ , and 10 SCCM  $\text{CH}_4$ , respectively. In doing so, thin film densification is avoided resulting in low acoustic impedance and moderate Young's moduli. The corresponding thin film at this focal point will from now be referred to as  $\text{a-SiOCN:H}$  with a mass density of only  $1.67 \text{ g/cm}^3$ .

The evolution of the precursor gas flow induced modification of the reference material system toward the focal point proved to be smooth in terms of both the mass density and the chemical matrix. This can be viewed by the comparison of the according *FT-IR* spectra in the so-called fingerprint region below  $1500 \text{ cm}^{-1}$  visible in Fig. 5.

The reference material system of  $\text{a-SiO}_2\text{:H}$  shows the typical behavior for silicon oxides with a main peak at  $1055 \text{ cm}^{-1}$  representing the Si-O network and the shoulder around higher wavenumbers for the Si-O cage structure. This ensemble for the oxide backbone is obviously weakened following the steady decrease of the  $\text{N}_2\text{O}$  flow and thereby also shifted to shorter wavenumbers. The decrease in Si-O bonds can also be viewed by the peak reduction at  $440 \text{ cm}^{-1}$ .<sup>19</sup> The presumably carbon-integrating ensemble arising below  $1000 \text{ cm}^{-1}$  consists of several overlapping peaks with obviously all sorts of bonds formed by Si, O, C, N, and H as involved elements. A further deconvolution into distinguishable bond peaks could not be achieved.

To quantify the development coming from the reference  $\text{a-SiO}_2\text{:H}$  and toward the focal point of  $\text{a-SiOCN:H}$ , quantities such as the *totally integrated area* and the *center of gravity (COG)* of the *absorption coefficient* within a wavenumber range of  $500\text{--}1350 \text{ cm}^{-1}$  is applied. The COG is hereby shifted from  $1076 \text{ cm}^{-1}$  ( $\text{a-SiO}_2\text{:H}$ ) down to  $974 \text{ cm}^{-1}$  for the focal point  $\text{a-SiOCN:H}$ , which strongly

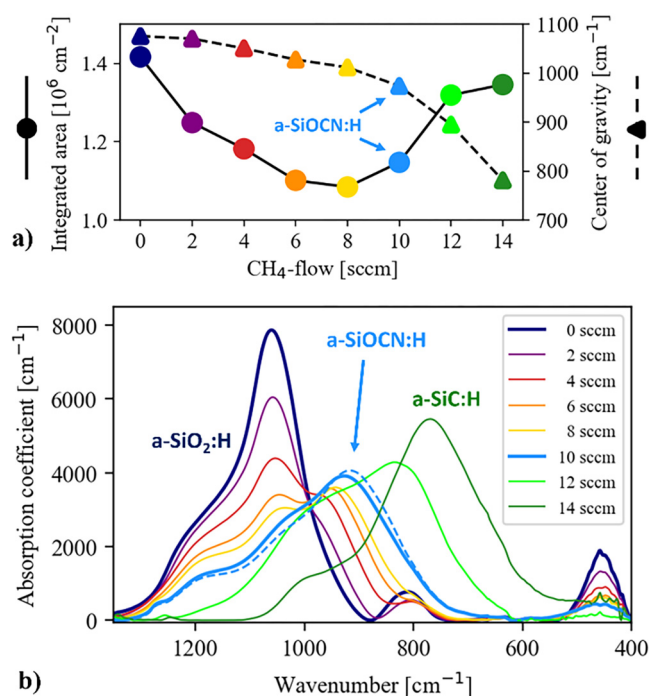


**FIG. 5.** FT-IR spectra evolving from the reference  $\text{a-SiO}_2\text{:H}$  through  $\text{a-SiOCN:H}$  and toward  $\text{a-SiC:H}$ . The typical cage and network ensemble of the oxide backbone is constantly decreasing when following the path as  $\text{N}_2\text{O}$  is exchanged by  $\text{CH}_4$ . Toward the focal point of optimum acoustic properties, the oxide-rich bond matrices are substituted by ensembles with presumably carbon-integrating structures, arising below  $1000 \text{ cm}^{-1}$ . In (a), the integrated area of the entire absorption coefficient spectra as a measure of the overall bond density within the thin films is illustrated. Furthermore, the center of gravity (COG) decreases with  $\text{CH}_4$  gas flow, which is a measure of bond agglomeration within the spectrum across all peaks. Both the total integrated area as well as the COG were applied in a range from  $500$  to  $1350 \text{ cm}^{-1}$ . Subplot (b) shows the respective FT-IR spectra. In addition, the *as-deposited* thin film spectrum of the focal point  $\text{a-SiOCN:H}$  is shown by the dashed line.

07 November 2024 11:08:36

indicates the bond modification in the matrix. If the *totally integrated area* is considered, it can be seen that for the targeted point of  $\text{a-SiOCN:H}$  there is only an amount of 81% of bonds left within the defined spectral range compared to the reference material system. This not only hints at a decreased bond concentration, in general but also underlines the lowered mass density of the material system at the focal point. Consider that the composition of 6 SCCM  $\text{SiH}_4$ , 6 SCCM  $\text{N}_2\text{O}$ , and 8 SCCM  $\text{CH}_4$  had an even lower figure of only 76.6% but accordingly a slightly higher mass density of  $\sim 1.69 \text{ g/cm}^3$ . For the compositions beyond the optimum point for low-Z, the thin films changed drastically, building up the denser matrix typical for  $\text{a-SiC:H}$ . The *totally integrated area* increased again, proving the absorption by a higher concentration of Si-C bonds.<sup>28</sup> The COG was strongly shifted toward lower wavenumbers stating the lack of reactive O atoms within the plasma, as can also be seen by the strong Si-C peak at  $770 \text{ cm}^{-1}$ . For the composition of  $\text{a-SiC:H}$ , the *totally integrated area* again reached closely

up to the value as for the reference material system, whereas the COG was then already below  $800\text{ cm}^{-1}$ .

An interesting result is the mentioned volume expansion by RTA for certain thin films in the range of moderate to high  $\text{CH}_4$  gas flows. This measurable effect by mass weighing and film thickness measurement can also be observed within the FT-IR spectra, as shown by the dashed line for the focal point a-SiOCN:H in Fig. 5. The *totally integrated area* for the *absorption coefficient* thereby decreased by roughly 1%, whereas the COG shifted to higher wavenumbers from  $965$  to  $974\text{ cm}^{-1}$ . Obviously, in the matrix of a-SiOCN:H, a higher content of oxide bonds formed during RTA, while losing an amount of carbon-integrating bonds between  $800$  and  $950\text{ cm}^{-1}$ . It can be assumed that the densification observed in thin films with high oxygen amount may be replaced within a-SiOCN:H by a healing effect of a bond structure incorporating Si, O, C, and even N and H, thus leading to thickness expansion and to the further decrease in mass density by RTA up to  $450^\circ\text{C}$ . This behavior of low-density a-SiOCN:H at the focal point when exposed to elevated temperatures is beneficial in comparison to the reference a-SiO<sub>2</sub>:H deposited by equal parameters, thus avoiding the decrease to dense oxide-rich structures (see Fig. 4). Interestingly, the thin film composition without any oxygen introduced by N<sub>2</sub>O, speaking of a-SiC:H, was not thermally influenced by RTA, indicating their temperature stability.

The obviously low ion energies in the plasma that are generated by the optimized deposition parameters lead to a substantial decrease in particle mobility, which is beneficial for the formation of low-density thin films. Moreover, through the substrate cooling to  $0^\circ\text{C}$  during thin film deposition, the particle mobility could be even further suppressed. Hence, the film growth is characterized by a small *deposition rate* with a resulting low-density microstructure. As the *deposition rate* for the reference material at standard parameters is above  $20\text{ nm/min}$ , that for the low-Z a-SiOCN:H was reduced to only to  $7.9\text{ nm/min}$ .

In opposition to the reference material system of a-SiO<sub>2</sub>:H, the composition at the focal point interestingly could be stated to be highly resistant against elevated temperatures up to the upper limit of  $450^\circ\text{C}$  both for the film thickness as well as for the mass density. This could be proven by mass weighing of the deposited a-SiOCN:H thin films pre- and post-*annealing*, with only a minor mass decrease within the measurement accuracy of less than 1%, whereas the film thickness even increased from  $474$  to  $490\text{ nm}$ , thereby further reducing the mass density from  $1.73$  to  $1.67\text{ g/cm}^3$  (see Fig. 4). In comparison, as mentioned before, the reference oxide collapsed in thickness during RTA and thereby changed from  $1.92\text{ g/cm}^3$  when *as-deposited* to a thermally stable version with a value of  $2.16\text{ g/cm}^3$  known to be close to standard oxides.<sup>32</sup>

To underline the low mass density of the low-Z a-SiOCN:H material system at the targeted focal point, the XRR measurement method confirmed a value of  $<1.7\text{ g/cm}^3$  after RTA. The critical angle where the grazing incidence x-ray beam is beginning to omit the total reflection behavior on the film surface and starts propagating into the thin film by  $0.33^\circ$  proved to be smaller in value than for known standard oxide obtained when the respective curve was fitted toward a SiO<sub>2</sub>-based model, see Fig. 6.

The other crucial property for acoustic impedance, *Young's modulus*, could be obtained to be on an increased level when

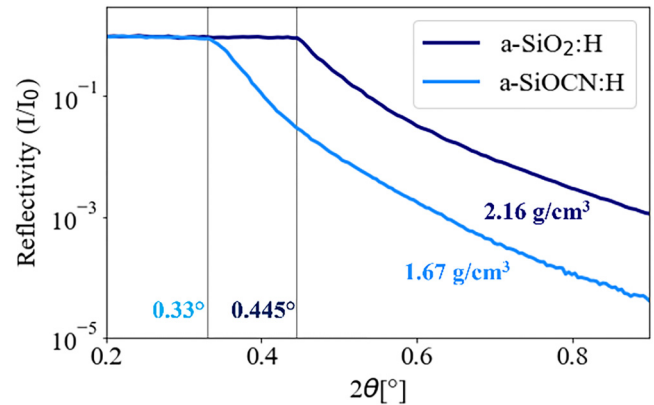


FIG. 6. X-ray reflectometry (XRR) curve with the double angle of total reflection  $2\theta$  fit to  $0.33^\circ$ , which corresponds to a mass density of  $<1.7\text{ g/cm}^3$ .

compared with prior works on SiOC.<sup>16</sup> Static measurements of *Young's modulus* by *nanindentation* directly proved the decrease from the reference material with  $78$  down to  $55\text{ GPa}$  for low-Z a-SiOCN:H when annealed and  $52\text{ GPa}$  for the *as-deposited* thin films. In Fig. 7, this result is illustrated in the characteristic curve fit.

However, the value obtained for *Young's modulus* was different from what was derived from the dynamic *picosecond ultrasonic* measurement for the sound velocity. The extracted value from the sound velocity measurement was lower when obtained and fitted to the according stack, described by Mason's model.<sup>33</sup> As a reference, typical values for PECVD a-SiO<sub>2</sub> found in the literature are in the range of  $5800$ – $6000\text{ m/s}$ ,<sup>8,34</sup> whereas the investigated low-Z a-SiOCN:H thin film of the focal point was proven to feature a decreased sound velocity  $v$  in the range of  $4180$ – $4190\text{ m/s}$ , see Fig. 8.

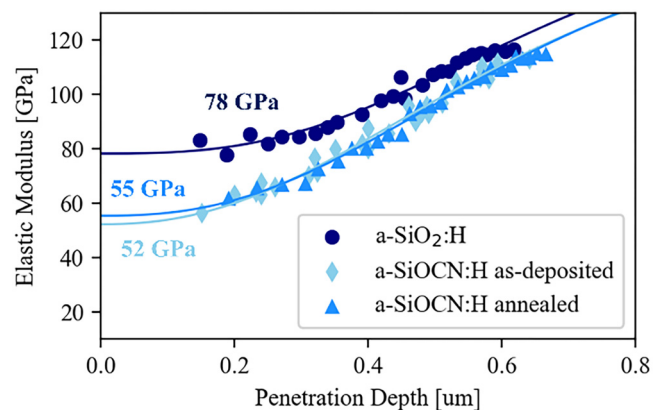
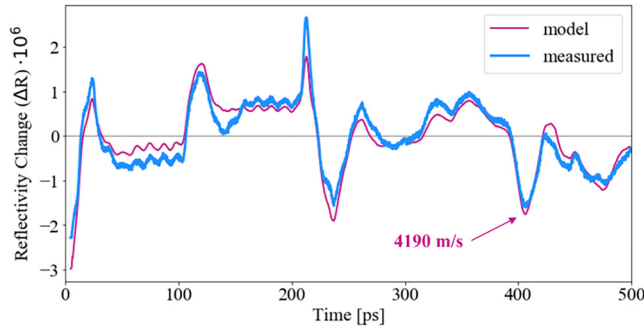


FIG. 7. Comparison of fitted nanoindentation curves (straight lines) by the Oliver–Pharr method from both the reference oxide (a-SiO<sub>2</sub>:H) as well as the low-Z a-SiOCN:H (annealed) thin film. The curve of the as-deposited a-SiOCN:H measured before RTA is also shown.

07 November 2024 11:08:36



**FIG. 8.** Picosecond ultrasonic measurement for the sound velocity of a-SiOCN:H. The applied Mason's<sup>33</sup> model of the low-Z thin film within the stack of Fig. 3 predicts a value of 4190 m/s. Accordingly, the measurement curve shows the exact same peak of reflection.

Together with the mass density obtained, a value of 30 GPa for *Young's modulus c* could be extracted by the simple terms of<sup>21</sup>

$$v = \sqrt{\frac{c}{\rho}}. \quad (3)$$

From this, a resulting acoustic impedance of 7.1 MRayl for low-Z a-SiOCN:H can be derived by (1). As mentioned before, the main advantage of SiO<sub>2</sub> vs the porous low-Z thin film materials is the higher sound velocity, which is directly dependent on *Young's modulus* compared to the known figures in this material class (SiOC, CDO, and OSG) and usually reaches 10–20 GPa for mass densities between 1.2 and 1.8 g/cm<sup>3</sup>.<sup>16</sup> However, as described in this work, tuning the deposition parameters according to Table I would enable the synthesization of less-dense a-SiOCN:H thin films in the range between 7 and 10 MRayl, with enhanced *Young's moduli* compared to porous low-Z thin films, thereby promising reduced viscous losses. The deposition of the precursor composition for nearly stoichiometric silicon carbide with 6 SCCM SiH<sub>4</sub> and 14 SCCM CH<sub>4</sub> led to a thin film with a similar low mass density of <1.7 g/cm<sup>3</sup> but showed static *Young's modulus* of 93 GPa, measured by *nanoindentation*. Hence, a wide range for tuning acoustic material properties is possible through the use of a-SiOCN:H, an important feature in accordance with integrated filter design.

A reasonable explanation for the difference in results between the *nanoindentation* method and *picosecond ultrasonic* can be attributed to how the amorphous, low-density material system reacts when stressed mechanically. During analysis with previous measurement technique, static compressive forces are applied, whereas the latter produces dynamic stress gradients when acoustic waves propagate through the material.

A highly important property for fabrication is the normalized residual film stresses of the focal point a-SiOCN:H deposition on a Si wafer calculated by (2). The resulting thin film stress was +80 MPa (tensile) for 700 nm films, thereby reducing to +63 MPa after the *annealing* step. This figure is only slightly higher than that for the reference a-SiO<sub>2</sub>:H with *as-deposited* +58 MPa at a comparable thickness. With these values for the

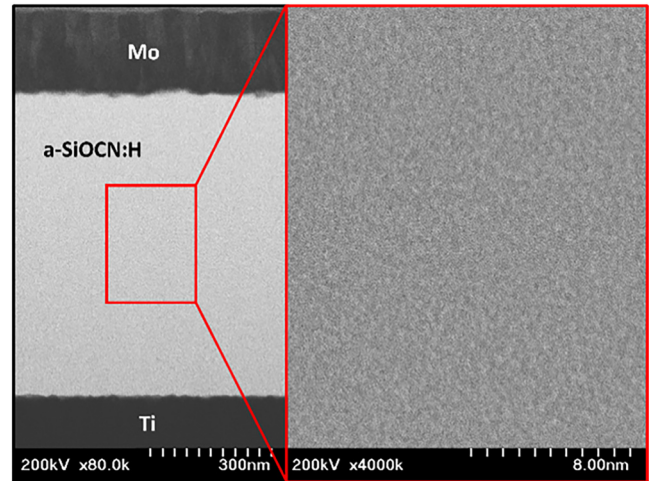


**FIG. 9.** Transmission electron microscopy (TEM) analysis of the a-SiOCN:H thin film at an acceleration voltage of 200 kV.

residual film stress, no severe complication should erupt during microfabrication.

Finally, the chemical composition of the a-SiOCN:H films is investigated, thus proving that the obtained material system belongs within the spectrum of prior low-Z thin film classes of SiOCs, CDOs, and OSGs. In prior works mentioned within the Introduction, structures with large pores that were intentionally formed within the thin films to reduce mass density always resulted in the disadvantageous property of weakening the mechanical elasticity.<sup>16</sup> As mentioned above, this common approach from low-k ILD research was avoided in this work to create a homogeneous low-density material system free of pores, see Fig. 9. The less-dense synthesized a-SiOCN:H thin films

07 November 2024 11:08:36

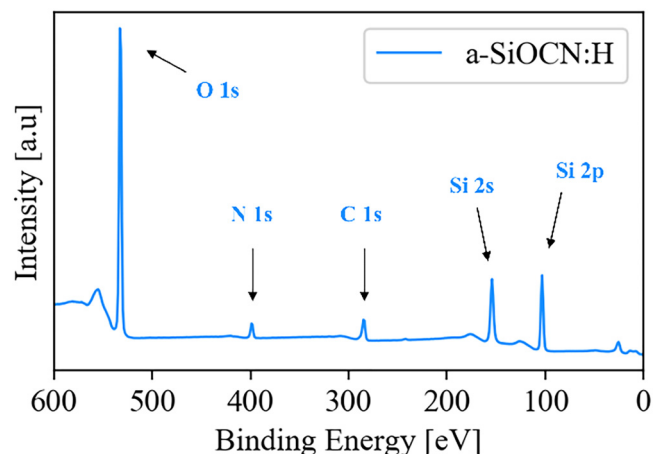


**FIG. 10.** X-ray photoelectron scattering (XPS) of the focal point a-SiOCN:H material system.

**TABLE II.** Elemental composition in at. [%] of a-SiOCN:H derived by XPS.

Element	at. %
Silicon (Si)	32.1
Oxygen (O)	52.5
Carbon (C)	11.3
Nitrogen (N)	4.1

offer an isotropic and homogeneous microstructure, thus preventing the disadvantageous effects of high viscous loss due to porosity from former SiOCs, CDOs, and OSGs, where large pores were rather voiding a continuous material structure.

In amorphous layers, various bonds depending on the number of elements used, their respective configuration of valence electrons, and the according atomic radii as well as bond lengths exist. As in prior SiO<sub>2</sub>, SiC, SiOC, CDO, or OSG compositions, hydrogen (-H) terminations introduced by precursors are omnipresent in PECVD layers.<sup>18,31,35</sup> These terminations occur with all sorts of atoms involved, to oxygen through the formation of hydroxyl groups (-OH), with nitrogen (-NH<sub>x</sub>) or silicon (-SiH<sub>x</sub>). Also methyl (-CH<sub>3</sub>) terminations<sup>31</sup> arise through the use of CH<sub>4</sub> as a precursor gas in a-SiOCN:H. This hydrogen incorporation within the material results in a low thin film density. On the other hand, the backbone structure of silicon bonds, consisting of Si-Si, Si-O, Si-C, and Si-N, is responsible for mechanical stability, and their respective ratio directly relates to the desired mechanical elasticity.

The elemental composition with the exception of hydrogen was determined by *X-ray photoelectron spectroscopy (XPS)*, see Fig. 10. Approximately one-third of the atoms comprises silicon, as it is also expected for highly stoichiometric a-SiO<sub>2</sub>. By introducing methane into the chamber by the amount of the composition in the focal point, the oxygen within the resulting thin films is reduced in favor of an increased carbon concentration. However, the simultaneous incorporation of a small amount of nitrogen atoms into the growing thin film occurs, originating from the N<sub>2</sub>O precursor. The exact elemental content is given in Table II.

#### IV. CONCLUSION

In this study, the synthesization of a-SiOCN:H thin films is proposed by applying a low-temperature PECVD process resulting in low-density layers without the presence of any detectable pores. With this material system, the opportunity for tailored acoustic properties is presented, following a different approach of precursor gas combination for simultaneous a-SiO<sub>2</sub>:H and a-SiC:H thin film deposition. The avoidance of pores and thereby the resulting isotropic, homogeneous structure even on the nm-scale results in less-dense growth, thus addressing the trade-off between low acoustic impedance and high as possible elasticity represented by Young's modulus. As a consequence, this allows the realization of a decreased acoustic impedance down to 7.1 MRayl in comparison to standard SiO<sub>2</sub>, which is a parameter of utmost importance for high-performance Bragg mirrors integrated in BAW solidly mounted resonator devices. Shifting the precursor mixture toward CH<sub>4</sub> or N<sub>2</sub>O as well as the deposition parameters also gives the opportunity to tune

acoustic material properties in a certain range so that a mechanical elasticity of at least 30 GPa could be maintained. It is reasonable to assume that the overall higher bond diversity in a-SiOCN:H thin films compared to silicon oxide serving as reference leads to a decrease in mass density due to the absence of repeatable bond structures. Conclusively, a novel synthesization route for low acoustic a-SiOCN:H thin films is presented as having the potential to fill the need for CMOS-compatible, low acoustic layers in tomorrow's high-frequency BAW filter elements for 5G applications.

#### ACKNOWLEDGMENTS

The authors are thankful to RF360 Europe GmbH for providing metrology equipment as well as measurements and data analyses in *X-ray reflectometry (XRR)*, *X-ray photoelectron scattering (XPS)*, *transmission electron microscopy (TEM)*, and *picosecond ultrasonic*.

This work was supported by the COMET Centre ASSIC Austrian Smart Systems Integration Research Center funded by BMVIT, BMDW, and the Austrian provinces of Carinthia and Styria, within the framework of COMET—Competence Centres for Excellent Technologies. The COMET programme is run by FFG.

#### AUTHOR DECLARATIONS

##### Conflict of Interest

The authors have no conflicts to disclose.

##### Author Contributions

**Claudio Berger:** Conceptualization (supporting); Data curation (lead); Formal analysis (lead); Investigation (lead); Methodology (lead); Visualization (lead); Writing – original draft (lead); Writing – review & editing (supporting). **Michael Schneider:** Conceptualization (lead); Funding acquisition (supporting); Methodology (supporting); Project administration (supporting); Resources (supporting); Writing – review & editing (supporting). **Georg Pfusterschmied:** Conceptualization (lead); Funding acquisition (supporting); Investigation (supporting); Methodology (supporting); Project administration (lead); Resources (supporting); Supervision (lead); Validation (lead); Writing – review & editing (lead). **Ulrich Schmid:** Conceptualization (lead); Funding acquisition (lead); Methodology (supporting); Project administration (supporting); Resources (lead); Supervision (lead); Validation (supporting); Writing – review & editing (lead).

#### DATA AVAILABILITY

The data that support the findings of this study are available from the corresponding author upon reasonable request.

#### REFERENCES

- <sup>1</sup>R. Aigner and G. Fattinger, “3G–4G–5G: How Baw filter technology enables a connected world,” in *2019 20th International Conference on Solid-State Sensors, Actuators and Microsystems Eurosensors XXXIII (TRANSDUCERS EUROSENSORS XXXIII)* (IEEE, 2019), pp. 523–526.
- <sup>2</sup>R. Aigner, G. Fattinger, M. Schaefer, K. Karnati, R. Rothmund, and F. Dumont, “BAW filters for 5G bands,” in *2018 IEEE International Electron Devices Meeting (IEDM)* (IEEE, 2018), pp. 14.5.1–14.5.4.

- <sup>3</sup>C. C. W. Ruppel, “Acoustic wave filter technology—A review,” *IEEE Trans. Ultrason. Ferroelectr. Freq. Control* **64**(9), 1390–1400 (2017).
- <sup>4</sup>A. Hagelauer, G. Fattinger, C. C. W. Ruppel, M. Ueda, K. Hashimoto, and A. Tag, “Microwave acoustic wave devices: Recent advances on architectures, modeling, materials, and packaging,” *IEEE Trans. Microw. Theory Tech.* **66**(10), 4548–4562 (2018).
- <sup>5</sup>R. Ruby, “11E-2 review and comparison of bulk acoustic wave FBAR, SMR technology,” in *2007 IEEE Ultrasonics Symposium Proceedings* (IEEE, 2007), pp. 1029–1040.
- <sup>6</sup>G. G. Fattinger, S. Marksteiner, J. Kaitila, and R. Aigner, “Optimization of acoustic dispersion for high performance thin film BAW resonators,” in *IEEE Ultrasonics Symposium, 2005* (IEEE, 2005), pp. 1175–1178.
- <sup>7</sup>S. Marksteiner, J. Kaitila, G. G. Fattinger, and R. Aigner, “Optimization of acoustic mirrors for solidly mounted BAW resonators,” in *IEEE Ultrasonics Symposium, 2005* (IEEE, 2005), pp. 329–332.
- <sup>8</sup>J. Olivares *et al.*, “Sputtered SiO<sub>2</sub> as low acoustic impedance material for Bragg mirror fabrication in BAW resonators,” *IEEE Trans. Ultrason. Ferroelectr. Freq. Control* **57**(1), 23–29 (2010).
- <sup>9</sup>J. Olivares, E. Wegmann, M. Clement, J. Capilla, E. Iborra, and J. Sangrador, “Wide bandwidth Bragg mirrors for multi-band filter chips,” in *2009 IEEE International Ultrasonics Symposium* (IEEE, 2009), pp. 2119–2122.
- <sup>10</sup>S. R. Gilbert, P. Nikkel, T. Jamneala, R. Ruby, J. D. Larson, and R. Thalhammer, “Improved coupled resonator filter performance using a carbon-doped oxide de-coupling layer,” in *2009 IEEE International Ultrasonics Symposium* (IEEE, 2009), pp. 867–871.
- <sup>11</sup>J. D. Larson and S. R. Gilbert, “Attenuation and velocity measurement at GHz frequencies in thin film carbon doped silicon oxide,” in *2010 IEEE International Ultrasonics Symposium* (IEEE, 2010), pp. 394–399.
- <sup>12</sup>T. Jamneala, M. Small, R. Ruby, and J. D. Larson, “Coupled resonator filter with single-layer acoustic coupler,” *IEEE Trans. Ultrason. Ferroelectr. Freq. Control* **55**(10), 2320–2326 (2008).
- <sup>13</sup>T. Jamneala *et al.*, “Ultra-miniature coupled resonator filter with single-layer acoustic coupler,” *IEEE Trans. Ultrason. Ferroelectr. Freq. Control* **56**(11), 2553–2558 (2009).
- <sup>14</sup>E. Iborra *et al.*, “BAW resonators based on AlN with Ir electrodes for digital wireless transmissions,” in *2008 IEEE Ultrasonics Symposium* (IEEE, 2008), pp. 2189–2192.
- <sup>15</sup>A. Reinhardt *et al.*, “P11-4 simulation of BAW resonators frequency adjustment,” in *2007 IEEE Ultrasonics Symposium Proceedings* (IEEE, 2007), pp. 1444–1447.
- <sup>16</sup>Y.-L. Cheng and C.-Y. Lee, “Porous low-dielectric-constant material for semiconductor microelectronics,” *Nanofluid Flow Porous Media* (published online 2018), Chap. 11.
- <sup>17</sup>M. R. Baklanov *et al.*, “Plasma processing of low-k dielectrics,” *J. Appl. Phys.* **113**(4), 041101 (2013).
- <sup>18</sup>W. Volksen, R. D. Miller, and G. Dubois, “Low dielectric constant materials,” *Chem. Rev.* **110**(1), 56–110 (2010).
- <sup>19</sup>A. Grill, S. M. Gates, T. E. Ryan, S. V. Nguyen, and D. Priyadarshini, “Progress in the development and understanding of advanced low k and ultralow k dielectrics for very large-scale integrated interconnects—State of the art,” *Appl. Phys. Rev.* **1**(1), 011306 (2014).
- <sup>20</sup>H. You *et al.*, “Extreme-low k porous pSiCOH dielectrics prepared by PECVD,” *J. Vac. Sci. Technol. B* **36**(1), 012202 (2018).
- <sup>21</sup>“Bulk Acoustic Wave Theory and Devices (Artech House Acoustics Library) by Joel Rosenbaum: Very Good (1988) | SecondSale.” Accessed Jun. 29, 2021 [Online], see <https://www.abebooks.com/Bulk-Acoustic-Wave-Theory-Devices-Artech/30923306228/bd>
- <sup>22</sup>W. C. Oliver and G. M. Pharr, “An improved technique for determining hardness and elastic modulus using load and displacement sensing indentation experiments,” *J. Mater. Res.* **7**(6), 1564–1583 (1992).
- <sup>23</sup>P. Emery, A. Devos, and P. Ancey, “Picosecond Ultrasonics: A Technique Destined for BAW Technology,” in *1st International Symposium on Laser Ultrasonics: Science, Technology and Applications, Montreal, Canada, 16–18 July 2008* (2008).
- <sup>24</sup>H. Maris, G. Antonelli, W. Ford, C. Morath, R. Stoner, and G. Tas, “Non-destructive testing using picosecond ultrasonics,” *AIP Conf. Proc.* **820**, 210–217 (2006).
- <sup>25</sup>G. G. Stoney and C. A. Parsons, “The tension of metallic films deposited by electrolysis,” *Proc. R. Soc. Lond. Ser. A* **82**(553), 172–175 (1909).
- <sup>26</sup>Y.-L. Cheng, Y.-L. Lin, C.-Y. Lee, G.-S. Chen, and J.-S. Fang, “Electrical characteristics and reliability of nitrogen-stuffed porous Low-k SiOCH/Mn<sub>2</sub>O<sub>3-x</sub>N/Cu integration,” *Molecules* **24**(21), 3882 (2019).
- <sup>27</sup>V.-A. Dao *et al.*, “Effect of N<sub>2</sub>O/SiH<sub>4</sub> flow ratios on properties of amorphous silicon oxide thin films deposited by inductively-coupled plasma chemical vapor deposition with application to silicon surface passivation,” *Vacuum* **84**(3), 410–414 (2009).
- <sup>28</sup>T. Frischmuth, M. Schneider, D. Maurer, T. Grille, and U. Schmid, “Inductively-coupled plasma-enhanced chemical vapour deposition of hydrogenated amorphous silicon carbide thin films for MEMS,” *Sens. Actuators A* **247**, 647–655 (2016).
- <sup>29</sup>T. Frischmuth, M. Schneider, D. Maurer, T. Grille, and U. Schmid, “High temperature annealing effects on the chemical and mechanical properties of inductively-coupled plasma-enhanced chemical vapor deposited a-SiC:H thin films,” *Thin Solid Films* **611**, 6–11 (2016).
- <sup>30</sup>T. Frischmuth *et al.*, “Low temperature deposition of a-SiC:H thin films applying a dual plasma source process,” *Thin Solid Films* **616**, 164–171 (2016).
- <sup>31</sup>D. Shamiryani, T. Abell, F. Iacopi, and K. Maex, “Low-k dielectric materials,” *Mater. Today* **7**(1), 34–39 (2004).
- <sup>32</sup>C. E. Viana, N. I. Morimoto, and O. Bonnaud, “Annealing effects in the PECVD SiO<sub>2</sub> thin films deposited using TEOS, Ar and O<sub>2</sub> mixture,” *Microelectron. Reliab.* **40**(4–5), 613–616 (2000).
- <sup>33</sup>J. V. Tirado, “Bulk acoustic wave resonators and their application to microwave devices.pdf.” Dissertation (Universitat Autònoma de Barcelona, 2010).
- <sup>34</sup>E. Nazaretski, R. D. Merithew, R. O. Pohl, and J. M. Parpia, “Measurement of the acoustic properties of amorphous silica above 4.5 mK,” *Phys. Rev. B* **71**(14), 144201 (2005).
- <sup>35</sup>K. Maex, M. R. Baklanov, D. Shamiryani, F. Iacopi, S. H. Brongersma, and Z. S. Yanovitskaya, “Low dielectric constant materials for microelectronics,” *J. Appl. Phys.* **93**(11), 8793–8841 (2003).